RSC Advances

PAPER

View Article Online
View Journal | View Issue

Cite this: *RSC Adv.*, 2021, **11**, 28211

Efficient visible-light photocatalytic H_2 evolution with heterostructured Ag_2S modified CdS nanowires†

Congrong Lu,‡[a] Shiwen Du,‡[b] Yanfei Zhao,[a] Qi Wang,[a] Kuankuan Ren,[a] Chunhe Li*[a] and Weidong Dou*[a]

Received 22nd June 2021
Accepted 17th August 2021

DOI: 10.1039/d1ra04823f

rsc.li/rsc-advances

The low separation efficiency of photogenerated charges and severe photocorrosion seriously impeded the application of CdS in photocatalytic water splitting. Here we report new routes to improve the photocatalytic performance of CdS nanowires (NWs) by decorating with Ag_2S nanoparticles, so Ag_2S/CdS heterojunction is constructed. The Ag_2S/CdS heterojunction exhibited optimal photocatalytic H_2 evolution rate of 777.3 μmol h^{-1} g^{-1}, which is 12.1 times higher than that of pure CdS. The intrinsic characteristics of Ag_2S/CdS nanocomposites, such as structure, optical properties, and surface chemical state are systematically studied by experimental characterizations and theoretical calculations. The comprehensive analysis demonstrates that the heterojunction between Ag_2S and CdS accelerates photoinduced electrons transfer from CdS to Ag_2S, enhancing their ability for water splitting. Meanwhile, the holes on the valence band of CdS react with the sacrificial agents, thus leading to the efficient separation of photogenerated electron–hole pairs. This work offers a simple route to synthesize one-dimensional CdS-based nanocomposites for efficient energy conversion driven by visible light.

1. Introduction

Water splitting for hydrogen evolution by semiconductor photocatalysts is one of the most promising solutions to alleviate the energy crisis. To improve solar-to-hydrogen energy conversion efficiency, numerous photocatalysts, such as TiO_2,[1] g-C_3N_4,[2] CdS,[3] ZnS,[4] $SrTiO_3$,[5] and so on, have been intensively studied over the last few decades. Especially, CdS is widely considered to be the most promising candidate in photocatalytic hydrogen evolution reaction (HER) due to its outstanding properties such as the proper band edge locations, moderate bandgap, and strong visible light absorption.

However, the high recombination rate of photogenerated charges and severe photocorrosion seriously hinder the application of CdS. Therefore, it is urgent to improve the electron–hole separation rate and enhance the photocatalytic stability for CdS. In recent years, one-dimensional (1D) nanostructured materials are extensively constructed because they have high aspect rations which are beneficial for H_2 evolution. It's well-known that 1D nanomaterials can accelerate the long-distance charge transfer velocity since 1D constructure provides a direct charge transport path along the axial direction for direct conduction.[6] In addition, the 1D materials can also enhance light-harvesting capacity and scattering properties which are substantially important for hydrogen evolution. As one of the outstanding examples of the 1D catalysts, CdS nanowires (NWs) have been successfully synthesized and used for photocatalytic HER. Nevertheless, the photocatalytic activity of CdS NWs is still unsatisfactory because of their poor reusability and depressed hydrogen production. Recently, it was demonstrated that the photocatalytic performance can be substantially improved by combining CdS with other cocatalysts including metal/alloy, metal phosphides, metal oxide/hydroxide, carbide, perovskite nanocrystals, metal sulfides, metal organic frame and so on. Especially, transition metal sulfides have attracted great attention owing to their unique optical, electrical, electrochemical, and other properties. For instance, 1D/2D CdS/CoS_x heterojunction was found to be very efficient for the hydrogen evolution;[7] CdS–MnS composite had very high stability which can maintain its catalytic ability for over 42 h of measurement,[8] MoS_2 NSs–CdS NWs system also possessed high visible-light H_2 evolution rate that far exceeded pure CdS NWs.[9]

As a typical transition metal sulfide, Ag_2S, with admirable photosensitive and low bandgap (0.9–1.2 eV),[10] was extensively used in binary or ternary photocatalysts, such as rGO/Ag_2S/g-C_3N_4,[11] CdS/Ag_2S/g-C_3N_4,[12] Ag_2S/ZnS,[13] and MoS_2/Ag_2S/Ag.[14] In addition, Ag_2S/CdS structure was also demonstrated to possess superior photocatalytic degradation performance under visible

[a]*Laboratory of Low-dimensional Carbon Materials, Department of Physics, Shaoxing University, Shaoxing 312000, China. E-mail: chunhe@whu.edu.cn; phyth@usx.edu.cn*
[b]*Dalian Institute of Chemical Physics, Chinese Academy of Sciences, Dalian National Laboratory for Clean Energy, Dalian 116023, China*

† Electronic supplementary information (ESI) available. See DOI: 10.1039/d1ra04823f

‡ These people contribute equally to this work.

light irradiation.[15] However, there are few reports on studying the influence of Ag_2S on CdS NWs in the photocatalytic hydrogen evolution.

In this work, we studied the photocatalytic HER activity of CdS NWs modified by Ag_2S nanoparticles (NPs) *via* a simple *in situ* ion exchange method. It was found that the 5.0%-Ag_2S/CdS exhibited optimal photocatalytic H_2 evolution rate of 777.3 μmol h^{-1} g^{-1}, which was 12.1 times higher than that of pure CdS NWs. The results exhibited that a heterojunction is formed at the interface between Ag_2S NPs and CdS NWs, and the co-catalyzed Ag_2S NPs provide active sites and trap photo-generated electrons, which results in efficient separation of "electron–hole" pairs. In addition, theoretical calculations based on density functional theory (DFT) were carried out to uncover the behind mechanism for the enhancement of photocatalytic activity. Our work demonstrates that Ag_2S NPs can be served as outstanding cocatalysts in the field photocatalytic HER from water splitting.

2. Experimental section

2.1. Chemicals

All chemical reagents are analytical grade and purchased from Aladdin Chemical Reagent Co., Ltd, AR. The ultrapure water (≥18 MΩ cm@25 °C) used in the whole experiment was purified from tap water in the laboratory.

2.2. Photocatalyst synthesis

(a) Synthesis of CdS NWs. CdS NWs were prepared by a facile solvothermal method which was reported in our previous work.[16]

(b) Synthesis of Ag_2S/CdS nanocomposites. The synthetic routes of Ag_2S NPs/CdS NWs nanocomposites are illustrated in Scheme 1. The Ag_2S/CdS composites were formed by the ion exchange between the CdS precursor and Ag^+. Typically, CdS NWs (1.445 g) were dispersed into 30 mL ultrapure water and then stirred for 30 min. After that, a certain amount of $AgNO_3$ was dissolved into the CdS NWs dispersion and vigorously stirred for another 30 min. The Ag_2S nanoparticles were *in situ* formed on the CdS surface, which can avoid the quick nucleation and growth of Ag_2S in the solution. It is expected that there are two main chemical reactions existing during the phase and morphological evolution, which are given as follows:

$$CdS \rightleftarrows Cd^{2+} + S^{2-} \quad (1)$$

$$2Ag^{+} + S^{2-} \rightleftarrows Ag_2S \quad (2)$$

As given in eqn (1), there is a small amount of S^{2-} in the reaction solution around the CdS nanowires, due to the dynamic equilibrium. When $AgNO_3$ was added in the suspension, nanosized Ag_2S particles were preferentially formed and deposited on the CdS surface by the heterogeneous nucleation (eqn (2)). The solubility product constant (K_{sp}) of CdS and Ag_2S is 8.0×10^{-27} and 6.3×10^{-50}, respectively.[17] Such large difference in solubility provides the driving force for cation exchange, forming the final Ag_2S/CdS composites.

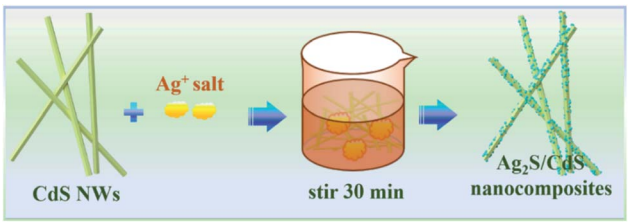

Scheme 1 Schematic illustration on the synthesis of Ag_2S/CdS nanocomposites.

Finally, the products were obtained by centrifugation, alternately rinsed with ultrapure water and ethanol several times, and dried at 60 °C for overnight. For comparison, the Ag_2S/CdS nanocomposites with various content of Ag_2S NPs were synthesized under the same condition. The ingredient molar rations of Ag_2S : CdS are 0.010, 0.025, 0.050 0.075, 0.100, and donated as 1.0%-Ag_2S/CdS, 2.5%-Ag_2S/CdS, 5.0%-Ag_2S/CdS, 7.5%-Ag_2S/CdS, and 10.0%-Ag_2S/CdS, respectively.

Details of characterization methods and parameters, photoelectrochemical parameters, photocatalytic H_2 evolution evaluation experiment, and theoretical calculation are available in the ESI.†

3. Results and discussions

3.1. Photocatalytic hydrogen evolution performance

The H_2 evolution performances of pure CdS and Ag_2S/CdS nanocomposites were evaluated under visible-light irradiation. Fig. 1a presented the cumulative H_2 production of the as-prepared samples. Intuitively, bare CdS shows a poor photocatalytic activity, which is attributed to the low separation efficiency of the photogenerated electron–hole pairs and serious photocorrosion. In contrast, the photocatalytic H_2 evolution activities of CdS are remarkably improved when composited with Ag_2S. It was found that the 5.0%-Ag_2S/CdS nanocomposite can produce hydrogen of 117.0 μmol after 3 h of irradiation, which is superior to the other samples. Fig. 1b listed the H_2 generation rate of all samples. It is clearly shown that the H_2 evolution rate of the Ag_2S/CdS nanocomposites gradually increases with the content of Ag_2S increasing from 1.0% to 5.0%, and achieves a maximum value of 777.3 μmol h^{-1} g^{-1} for the 5.0%-Ag_2S/CdS nanocomposite. This value is 12.1 times higher than that of pure CdS. Further increase of the Ag_2S content leads to the decrement of H_2 generation rate, which indicates that moderate content of Ag_2S in Ag_2S/CdS is needed for high performance of H_2 generation. Although Ag_2S NPs offer abundant surface hydrogen evolution active sites, excessive Ag_2S cause severe aggregation and shielding effect for light absorption, which may result in the depression of photocatalytic activity.

3.2. Structural analysis

In order to understand the influence of the structure of the catalysts on their photocatalytic HER performance, X-ray diffractometer (XRD) measurements were performed to detect

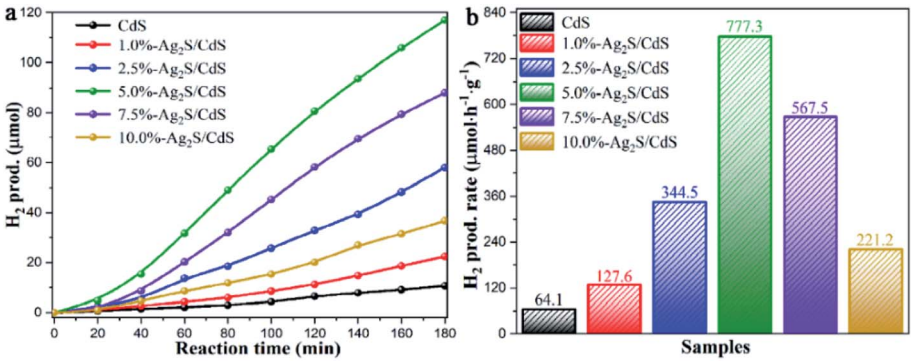

Fig. 1 (a) Time courses of photocatalytic H_2 production; and (b) comparison of the H_2 generation rate of samples over CdS and Ag_2S/CdS nanocomposites under visible light irradiation.

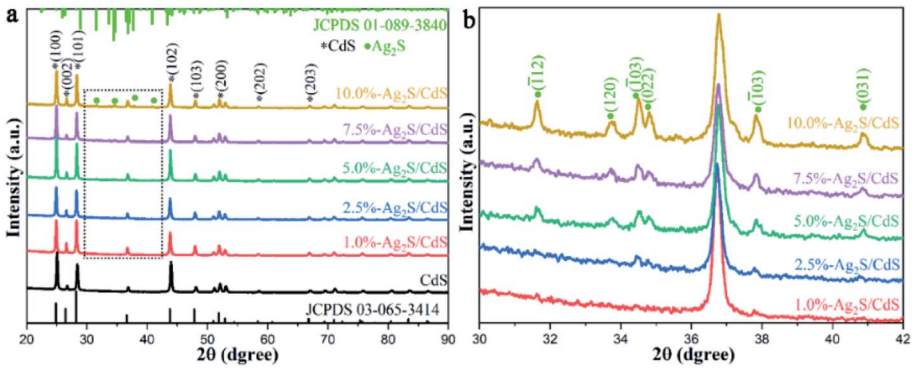

Fig. 2 (a and b) XRD patterns XRD patterns of CdS, and Ag_2S/CdS nanocomposites.

the crystal structures of pure CdS and Ag_2S/CdS nanocomposites. As shown in Fig. 2a, it is obvious that the sharp and strong characteristic diffraction peaks located at 24.9°, 26.5°, 28.2°, 36.6°, 47.8°, 51.0°, 58.4°, and 66.8° belong to the (100), (002), (101), (102), (103), (200), (202), and (203) planes of hexagonal CdS with high crystallinity (JCPDS no. 03-065-3414), respectively.[18] In addition to the diffraction peaks of pristine CdS, some new peaks at 31.5°, 33.7°, 34.4°, 34.7°, 37.7°, and 40.8° were also observed in the XRD patterns of (2.5%, 5.0%, 7.5%, 10%)-Ag_2S/CdS nanocomposites (Fig. 2b). These peaks can be ascribed to the ($\bar{1}$12), (120), ($\bar{1}$21), (022), ($\bar{1}$03), and (031) faces of monoclinic Ag_2S (JCPDS no. 01-089-3840), respectively.[19] This observation demonstrated that Ag_2S has been successfully loaded onto CdS. However, the characteristic diffraction peaks of Ag_2S are hardly identified in the XRD data of 1.0%-Ag_2S/CdS nanocomposite which may due to the low content of Ag_2S in the Ag_2S/CdS nanocomposites. Therefore, it is necessary to further prove the existence of Ag_2S in Ag_2S/CdS nanocomposite by other characterization techniques.

To gain deep insight into the morphology and structure of CdS and Ag_2S/CdS nanocomposites, the scanning electron microscopy (SEM) images were obtained. As shown in Fig. 3a, the morphology of a single CdS displays nanowire with approximately 5 μm in length and has a clean and smooth surface. Compared with the smooth surface of CdS NWs, the Ag_2S/CdS nanocomposites remain uniform nanowires, except the covering with more and more nano-scaled nanoparticles on their surfaces, as the molar ratio of Ag_2S to CdS increasing from 1.0% to 10.0% (Fig. 3a–f). Fig. 3(d_1–d_3) display the special distribution of Cd, S, and Ag elements for the sample of 5.0%-Ag_2S/CdS nanocomposite. The distribution of these elements is quite uniform and agrees with the shape of CdS NW, indicating that Ag_2S NPs have well adhered onto the surface of CdS NWs. Simultaneously, the SEM results indicate the *in situ* ion exchange process of Ag^+ is an effective method to construct Ag_2S-based cocatalyst.[20]

To further demonstrate the existence of Ag_2S NPs on the surface of CdS NWs, transmission electron microscopy (TEM) was used to characterize the details of CdS NWs and 5.0%-Ag_2S/CdS nanocomposite. As shown in Fig. 4a, pure CdS NWs display a smooth surface with approximately 64 nm in diameter. This indicates that the aspect ratio of CdS NWs is quite high. This observation agrees well with the SEM measurements as mentioned above. And the large aspect ratio of CdS NW provides a high-speed channel for carrier transmission during photocatalytic process. Fig. 4b shows the high-resolution TEM (HRTEM) image of CdS NW. The interplanar distance between two adjacent crystal planes is measured to be 2.45 Å which is agreed well with the interlayer distance of (102) plane of CdS (Fig. 4b, b_1 and b_2). Fig. 4c shows the low-magnified TEM image

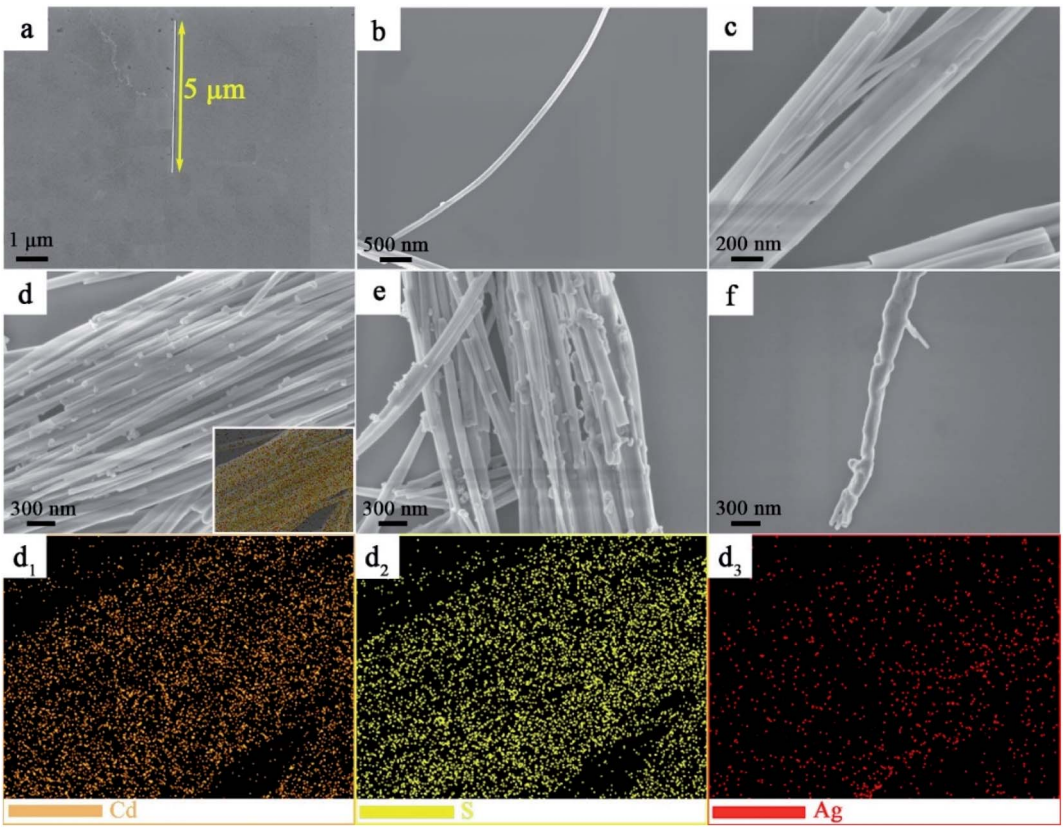

Fig. 3 SEM images of various samples: (a) CdS, (b) 1.0%-Ag_2S/CdS, (c) 2.5%-Ag_2S/CdS, (d) 5.0%-Ag_2S/CdS, (e) 7.5%-Ag_2S/CdS, (f) 10.0%-Ag_2S/CdS, and (d_1–d_3) corresponding elemental mappings showing the ordered distribution of (d).

of 5.0%-Ag_2S/CdS nanocomposite for which the morphology is quite different to that of pure CdS NWs. It clearly shows that some irregular particles with sizes ranging from 20 to 80 nm are randomly located on the surface of CdS NWs for the 5.0%-Ag_2S/CdS nanocomposite (Fig. 4c). Fig. 4d shows the HRTEM images of 5.0%-Ag_2S/CdS, the *d*-spacing fringes of 2.45 Å and 2.05 Å are in good agreement with CdS (102) and Ag_2S (103) plane, respectively. In addition, the consecutive lattice fringes between CdS NWs, and Ag_2S NPs manifest the formation of desirable heterojunction structure at their interfaces.

Fig. 5 shows nitrogen adsorption–desorption isotherms and the corresponding pore-size distribution curves of pure CdS, 5.0%-Ag_2S/CdS, and 10.0%-Ag_2S/CdS nanocomposites. As shown in Fig. 5a, it can be seen that the nitrogen adsorption–desorption isotherms for these three samples are type IV with hysteresis H3 hysteresis loops at the P/P_0 range of 0.7–1.0 according to the IUPAC classification, indicating the existence of mesopores and large macropores.[21] The BET specific surface areas, pore volumes, and average pore sizes of all of the samples are summarized in Table 1. The BET specific surface area (S_{BET}) of the pure CdS nanowires is about 60.79 $m^2\ g^{-1}$. After 5.0% Ag_2S is coated the S_{BET} of 5.0%-Ag_2S/CdS increased to 65.15 $m^2\ g^{-1}$. This is because the irregular Ag_2S nanoparticles grow on the surface of the CdS NWs, resulting in expanded surface area. It was well-recognized that the large surface area contributes to absorbing more active species and reactants on its surface, which is beneficial to effectively promoting the photocatalytic reaction.

As can be seen in the inset of Fig. 5b, the pristine CdS nanowires contain both mesopores (2–50 nm) and macropores (50–100 nm). The presence of small amount of Ag_2S (5.0%) can introduce a lot of mesopores (2–50 nm) and thus decrease the pore volumes, and average pore sizes. However, for 10.0%-Ag_2S/CdS, the further increase of the Ag_2S content (from 5.0% to 10.0%) may lead to the adhesion and aggregation excessively of Ag_2S on the CdS surface, which in turn reduces S_{BET} and pore volumes. This analysis is in accordance with the SEM results.

Fig. 6a displayed the UV-vis diffuse reflectance spectrometer (DRS) of CdS NWs and Ag_2S/CdS nanocomposites, which has been extensively used to evaluate the optical properties of semiconductor photocatalysts. It is worth noting that the attachment of Ag_2S NPs on CdS NW usually causes the narrowing of the band gap. This effect results in the red shift of the cutting edge in UV-vis spectra compared with pure CdS NWs. According to Kubelka–Munk function *vs.* the band-gap energy, the absorption edge of pure CdS NWs and 5.0%-Ag_2S/CdS nanocomposite are located at 518 nm and 533 nm, which corresponds to a bandgap of *ca.* 2.39 eV and 2.33 eV. Besides, with the increment of Ag_2S content, the absorption intensity of the Ag_2S/CdS nanocomposites increase simultaneously in visible and near-infrared regions (520–1000 nm). The narrowed band-gap and increased absorption intensity of Ag_2S/CdS

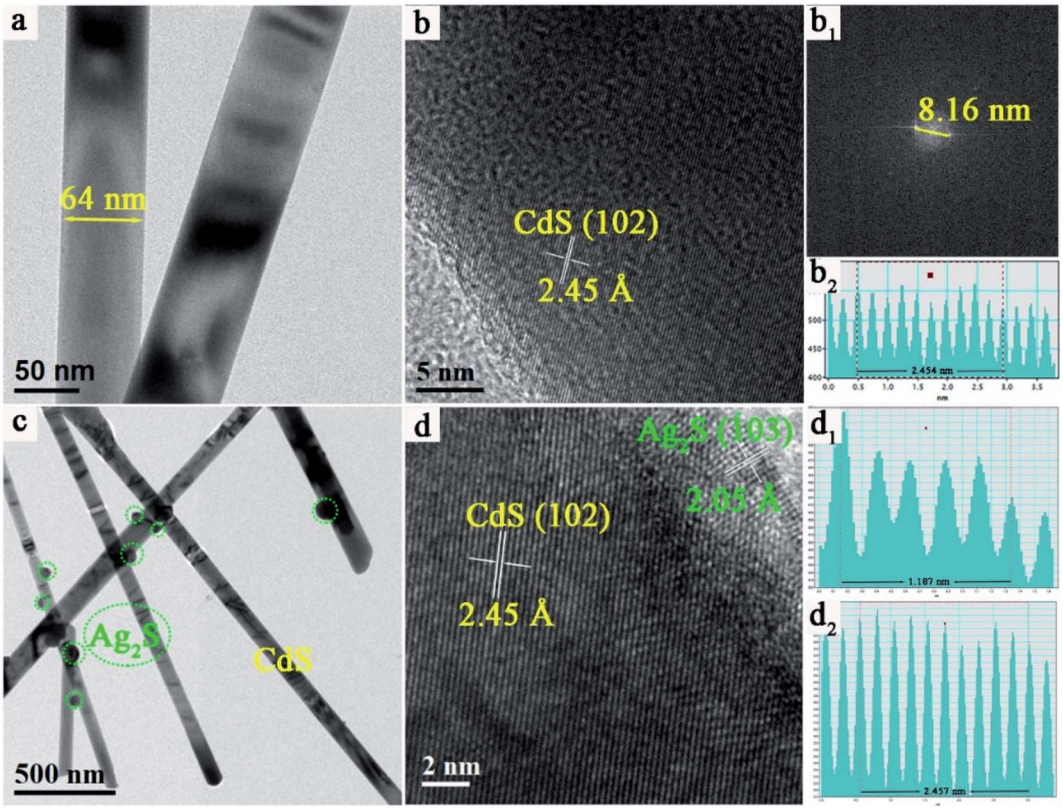

Fig. 4 (a and b) TEM/HRTEM results of CdS NWs, (b_1) corresponding FFT patterns of (b) and (b_2) profile plots of the calibration for measured the interplanar distance of CdS; (c and d) TEM/HRTEM images of 5.0%-Ag_2S/CdS nanocomposite and (d_1 and d_2) profile plots of the calibration for measured the interplanar distance of CdS and Ag_2S in (d).

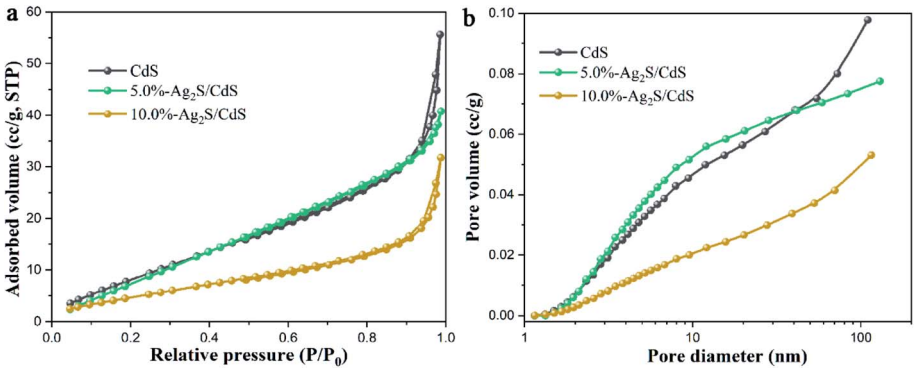

Fig. 5 (a) N_2 adsorption–desorption isotherms; and (b) the corresponding pore size distribution curves of CdS, 5.0%-Ag_2S/CdS, and 10.0%-Ag_2S/CdS.

nanocomposites can be ascribed to the formation of heterojunction and the high absorption cross section of Ag_2S NPs (Fig. 6b).[22,23] These observations indicate that these nanocomposites can produce photoexcited electron–hole pairs under visible light irradiation, thus triggering consecutive chemical redox reactions.

To further investigate the surface chemical state and bonding configuration of samples, X-ray photoelectron spectroscopy (XPS) analysis was employed. As shown in Fig. 7a, both CdS and 5.0%-Ag_2S/CdS nanocomposite contain Cd, S, O and C elements. In addition, the characteristic peak of Ag was also detected, suggesting the existence of Ag_2S in the Ag_2S/CdS nanocomposite. Fig. 7b denoted the Cd 3d spectra of CdS and 5.0%-Ag_2S/CdS nanocomposite, the two main peaks centered at 404.5 eV and 411.3 eV were thoroughly deconvolved into Cd $3d_{5/2}$ and Cd $3d_{3/2}$ of Cd^{2+}, respectively. In Fig. 7c, the binding energies at 161.0 eV and 162.2 eV for pure CdS, and at 161.6 eV and 162.2 eV for 5.0%-Ag_2S/CdS nanocomposite are indexed to S $2p_{3/2}$ and S $2p_{1/2}$ spin–orbit for S^{2-}, respectively. The corresponding peaks of S 2p for 5.0%-Ag_2S/CdS nanocomposite

Table 1 The S_{BET}, pore volume, and average pore size of pure CdS nanowires and NiS/CdS nanocomposites

Sample	S_{BET} ($m^2\ g^{-1}$)	Pore volume ($cm^3\ g^{-1}$)	Average pore size (nm)
CdS	60.79	0.10	2.32
5.0%-Ag_2S/CdS	65.14	0.08	2.10
10.0%-Ag_2S/CdS	27.35	0.05	2.11

moved slightly toward higher binding energy than those of pure CdS. The shifting of peak positions may origin from the intimate interaction between Ag_2S and CdS, which can result in the change in electron concentration on the surface of the photocatalysts. As given in Fig. 7d, two peaks located at 367.8 eV and 373.5 eV of 5.0%-Ag_2S/CdS nanocomposite could be ascribed to the Ag $3d_{5/2}$ and Ag $3d_{3/2}$ of Ag^+, respectively.[24] The above XPS results further manifest the coexistence of CdS and Ag_2S in 5.0%-Ag_2S/CdS nanocomposite. Meanwhile, a heterojunction as

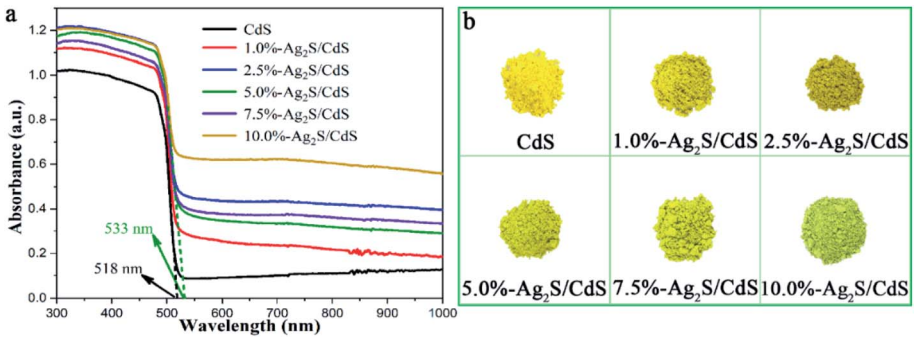

Fig. 6 (a) UV-vis DRS and (b) corresponding images of CdS and Ag_2S/CdS nanocomposites.

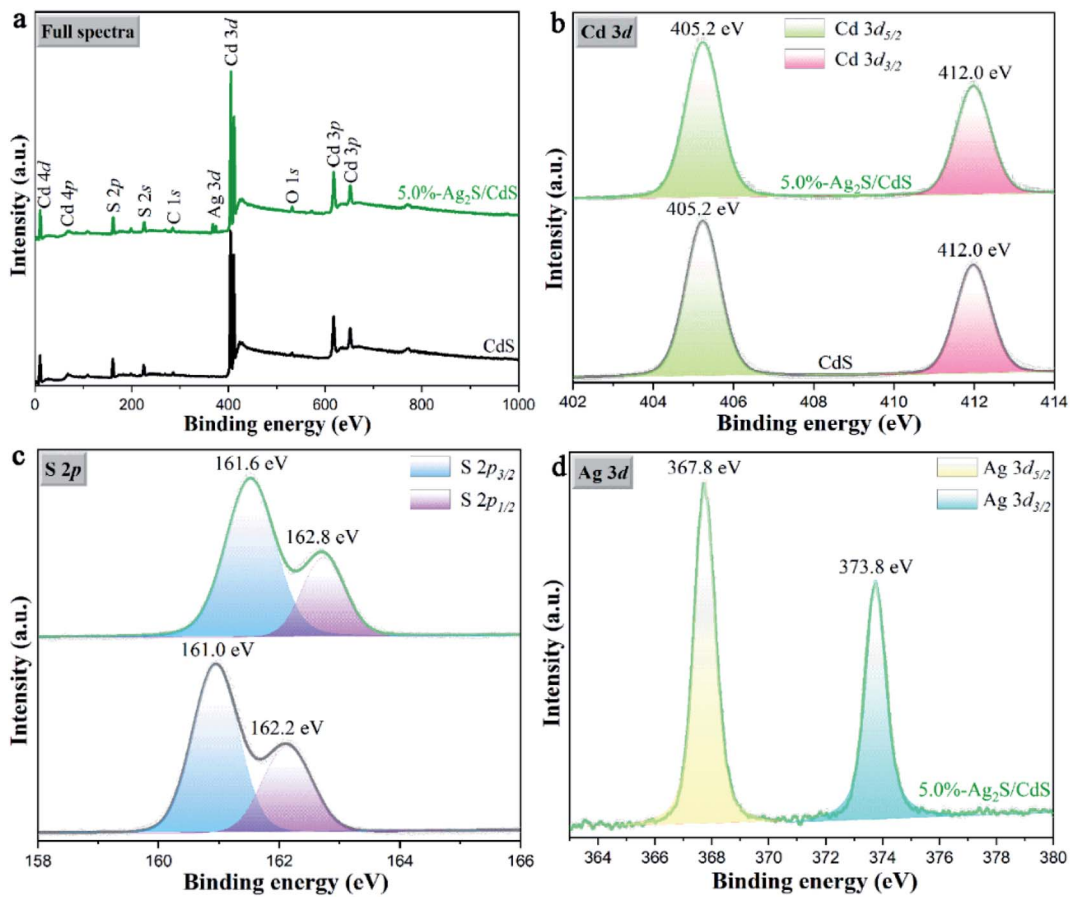

Fig. 7 (a) Full XPS survey spectra; and high-resolution XPS spectra of (b) Cd 3d, (c) S 2p and (d) Ag 3d of the CdS and 5.0%-Ag_2S/CdS nanocomposite.

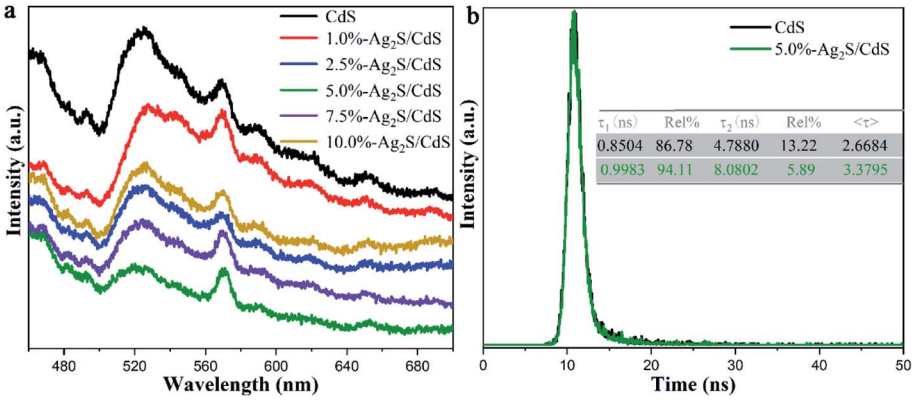

Fig. 8 (a) Steady-state PL spectra of CdS and Ag_2S/CdS nanocomposites; and (b) TRPL decay of CdS and 5.0%-Ag_2S/CdS nanocomposites at an excitation wavelength of 525 nm.

being demonstrated by the HRTEM images shown in Fig. 5 is formed at the interface of the two components.

3.3. Photoelectric performance characterization

It is well-known that photoluminescence (PL) spectra can provide the information on separation and transfer process of photogenerated charge carriers. We carried out PL measurements to investigate the carrier behavior of CdS and Ag_2S/CdS nanocomposites. The low PL intensity indicates a high electron–hole separation rate and excellent photocatalytic performance.[25] Fig. 8a is the steady-state PL spectra of all samples using an excitation wavelength of 380 nm, and two obvious emission peaks at about 525 and 570 nm appeared. The emission peak at 525 nm is assigned to the near-band-gap transition in CdS, and the other emission peak at 570 nm is due to the recombination of the electron–hole pairs near the surface of the photocatalysts.[26] It is worth noting that the peak intensity at 570 nm is strong. This phenomenon is ascribed to the long wire-like of CdS. Liu *et al.* discovered that the area of exposed nonpolar surface and degree of surface defects increase with an increase in aspect ratio.[27] In our work, the aspect ratio (~78) of long CdS nanowire is quite high, which means there is abundant surface defects on the surface of CdS. These surface defects can trap photo-induced electrons/holes, and thus decrease their probability of recombination. Meanwhile, compared with pure CdS, the PL spectra of Ag_2S/CdS nanocomposites show similar but with weaker intensity, indicating their high-efficiency of photogenerated electron–hole separation. Among them, 5.0%-Ag_2S/CdS nanocomposite shows the weakest PL spectral intensity, illustrating that the most efficient separation rate of photogenerated electrons and holes by the heterojunction effect between Ag_2S and CdS.

Furthermore, the time-resolved photoluminescence (TRPL) character (Fig. 8b) of pure CdS and 5.0%-Ag_2S/CdS nanocomposite were recorded to track the photo-physical behavior of charge carriers. The fluorescent decay profiles of both samples can be well fitted by two exponential terms, and their average lifetime was obtained according to the following equations:[28,29]

$$\langle\tau\rangle = \frac{B_1\,\tau_1{}^2 + B_2\,\tau_2{}^2}{B_1\tau_1 + B_2\tau_2} \quad (3)$$

where $\langle\tau\rangle$, $\tau_{i=1,2}$, and $B_{i=1,2}$ refer to the average lifetime, the decay time of the individual components, the corresponding amplitudes, respectively. Specially, the shorter lifetime, τ_1, increased from 0.08504 ns for pure CdS to 0.9983 ns for 5.0%-Ag_2S/CdS nanocomposite. In addition, the corresponding component increased from 86.78% to 94.11%. The longer lifetime, τ_2 of 5.0%-Ag_2S/CdS nanocomposite was increased to 8.0802 ns, but its component decreased from 13.22% to 5.89%. Using these parameters, an averaged lifetime of *ca.* 3.3795 ns for the sample of 5.0%-Ag_2S/CdS nanocomposite, which is remarkably longer than that of pure CdS NWs (2.6684 ns). The prolonged lifetime is closely related to the acceleration of electron transport, which can boost the probability of photoinduced electrons and holes participating in photo-redox process.

Electrochemical analysis such as transient photocurrent response, electrochemical impedance spectroscopy (EIS) Nyquist plots, linear sweep voltammetry (LSV), and Mott–Schottky plots were carried out to analyze the photogenerated carriers transfer properties of CdS and Ag_2S/CdS nanocomposites. The transient photocurrent–time curves were measured by switching the irradiation light on–off for several runs. As displayed in Fig. 9a, a notable rise in the photoelectric response formed for all samples, indicating the high response of photoinduced electrons under visible-light stimulation. However, pure CdS shows a very weak photocurrent due to the fast electron–hole pairs recombination. And the photocurrent density becomes almost undetectable after several cycles of light stimulation due to the photocorrosion effect. In contrast, Ag_2S/CdS samples show much higher photocurrent intensity and more reliable stability than that of pure CdS NW. We found that the sample of 5.0%-Ag_2S/CdS nanocomposite shows the strongest photocurrent. This implies that the sample of 5.0%-Ag_2S/CdS is most efficient for the photogenerated electron–hole pairs separation. This observation is consistent with PL spectra mentioned above.

To explore the influence of Ag_2S on the electronic transport dynamics of CdS, EIS measurements are performed (Fig. 9b). The arc radius of Ag_2S/CdS nanocomposites in the Nyquist plots are smaller than that of CdS, which indicates that the charge transfer resistance of Ag_2S/CdS nanocomposites is lower than that of CdS, meaning the faster interfacial charge separation for

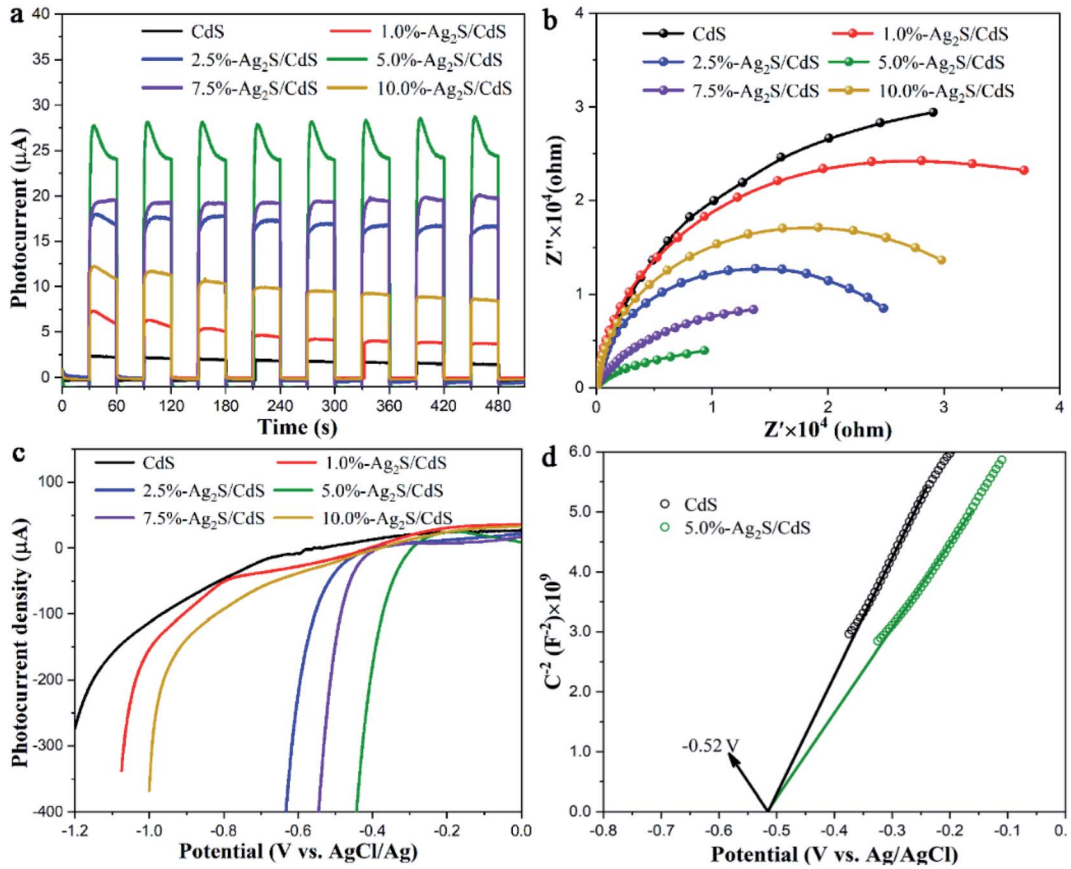

Fig. 9 (a) Transient photocurrent response; (b) EIS Nyquist plots; (c) LSV of CdS and Ag_2S/CdS nanocomposites; (d) Mott–Schottky plots of CdS and 5.0%-Ag_2S/CdS nanocomposites.

the Ag_2S/CdS nanocomposites. Concurrently, the 5.0%-Ag_2S/CdS nanocomposite exhibited the smallest semicircle, implying that moderate Ag_2S nanoparticles on CdS NWs can effectively enhance the charge separation efficiency.

To identify the key roles of Ag_2S in improving the photocatalytic HER process, the polarization curves of CdS and Ag_2S/CdS nanocomposites were also investigated. As shown in Fig. 9c, compared to the other samples, 5.0%-Ag_2S/CdS nanocomposite had the lowest overpotential. Since the photocatalytic performance is closely related to overpotential,[30] the LSV results further support our conclusion that 5.0%-Ag_2S/CdS nanocomposite is an excellent photocatalyst for HER. The results are in accordance with the photocatalytic activity and PL analysis.

Mott–Schottky experiment was applied to evaluate the carrier density and band positions of the CdS and 5.0%-Ag_2S/CdS nanocomposite. As presented in Fig. 9d, the positive slope of C^{-2} *vs.* E plot indicates that both samples are n-type semiconductors.[31] And the carrier density can be calculated through taking the slope of the linear part in the Mott–Schottky plots into the following equation:

$$N_d = \frac{2}{\varepsilon\varepsilon_0 q}\left[\frac{d\left(\frac{1}{C^2}\right)}{dV}\right]^{-1} \quad (4)$$

Here, N_d is the carrier density, ε is the dielectric constant of Ag_2S (7.77) and CdS (8.7), ε_0 (8.854×10^{-12} F m^{-1}) is the vacuum permittivity, q (1.603×10^{-19} C) is the electron charge, and V is the potential applied at the electrode, respectively. Using these parameters, the N_d were calculated as 8.29×10^{14} cm^{-3} and 1.15×10^{15} cm^{-3} for CdS and 5.0%-Ag_2S/CdS nanocomposite, respectively. It's obvious that the electron density in the 5.0%-Ag_2S/CdS nanocomposite much higher than that of CdS. This property can undoubtedly enhance H_2 evolution activity for Ag_2S/CdS nanocomposites.

3.4. Photocatalytic mechanism

In order to understand the electron transfer between CdS and Ag_2S in Ag_2S/CdS nanocomposites, the work functions (W_F) of CdS and Ag_2S were obtained in terms of the UPS spectra. And the work function value was calculated in accordance with the following equation:

$$W_F = h\nu - E_{cut\text{-}off} \quad (5)$$

where $h\nu = 21.22$ eV, $E_{cut\text{-}off}$ is the cut-off edge of the secondary electrons in samples. As shown in Fig. 10a, the $E_{cut\text{-}off}$ of CdS and Ag_2S are 16.97 eV and 16.73 eV, respectively. According to the eqn (5), the calculated W_F of CdS and Ag_2S are 4.25 eV and 4.48 eV, respectively. The corresponding schematic diagram of the energy band structures energy band structures about CdS and Ag_2S are shown in Fig. 10b. Ag_2S displays a relatively lower Fermi level than that of CdS. When CdS and Ag_2S come into

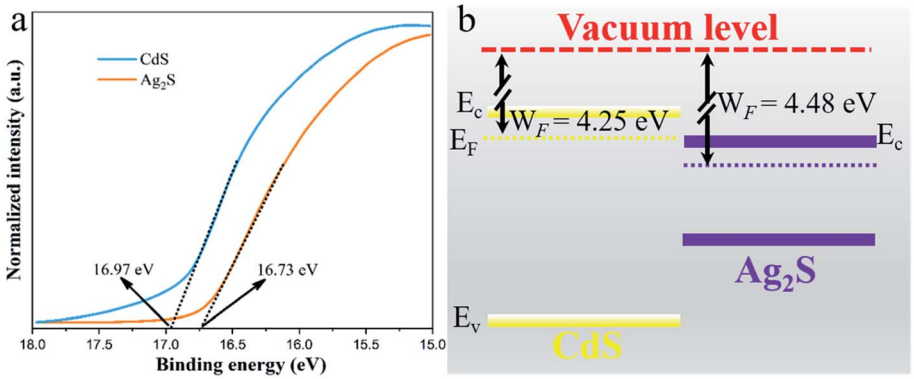

Fig. 10 (a) Ultraviolet photoelectron spectroscopy (UPS) spectra; and (b) the schematics of the energy band position of CdS and Ag_2S.

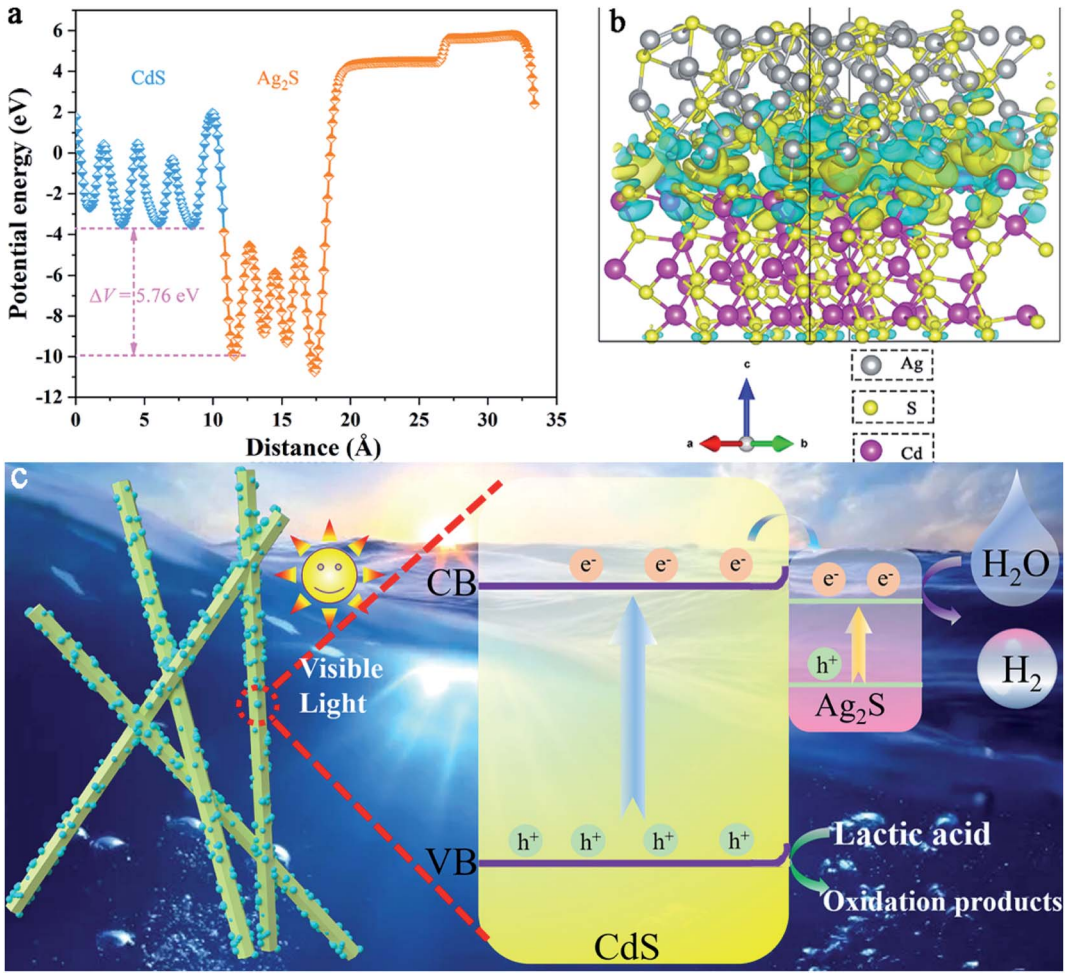

Fig. 11 (a) Potential drop across the interface; (b) the charge difference of Ag_2S/CdS nanocomposites; (c) photocatalytic mechanism of H_2 generation with Ag_2S/CdS composites.

contact, the electrons will diffuse from CdS to Ag_2S to build up an equilibrium state between their Fermi levels.[32,33] The result indicates that there is a built-in electric field at the interface between CdS and Ag_2S, and the conduction band position of Ag_2S move upward to a more negative position. Thus, the photogenerated electrons in CdS tend to flow from CdS to Ag_2S, and then participate in the photocatalytic H_2 production from water splitting.

In addition, to better understand the charge transfer mechanism between the Ag_2S/CdS nanocomposites, some theoretical calculations were carried out.[34,35] As shown in Fig. 11a, the potential drop (ΔV) across the Ag_2S/CdS interface is 5.76 eV,

leading to the formation of a built-in electric field from the Ag_2S to the CdS. This built-in electric field is a key factor to enhances the separation of photogenerated electron–hole pairs. Fig. 11b gives the charge density difference of Ag_2S/CdS nanocomposites. The cyan region and yellow region stand for charge depletion and accumulation near the heterojunction interface, respectively. It is found that both electrons and holes are located at the interface region of the Ag_2S/CdS, forming well-separated electron depletion and accumulation region, which is beneficial for the separation of electron–hole pairs.[36,37]

The flat-band potential (V_{fb}) of pure CdS was obtained by extrapolating tangent to the *X*-intercept in the Mott–Schottky curve (Fig. 9b). It is worth mentioning that the introduction of Ag_2S does not alter the band structure of CdS. Both the V_{fb} of CdS and 5.0%-Ag_2S/CdS nanocomposite were about −0.63 V *vs.* Ag/AgCl. Usually, the bottom of the conduction bands (CB) is more negative than the flat band potential for many n-type semiconductors. According to the transformation relation formula between Ag/AgCl electrode and normal hydrogen electrode (NHE): $E_{NHE} = E_{Ag/AgCl} + 0.197$ and DRS results, the CB and valence band (VB) of CdS were −0.73 V and 1.66 V *vs.* NHE, respectively. According to the previous reports, the CB and VB of Ag_2S are about −0.23 and 0.69 V *vs.* NHE, respectively. Based on the above analysis, a photocatalytic mechanism of hydrogen generation with Ag_2S/CdS composites is proposed (Fig. 11c). Under visible light irradiation, both CdS and Ag_2S samples are simultaneously excited to produce photogenerated electrons and holes. Meanwhile, the CB of CdS is more negative than that of Ag_2S, the photogenerated electrons in the CB of CdS can be rapidly migrated to the conduction band of Ag_2S. Thus, these can participate in HER through the abundant active sites in Ag_2S. These results confirm that the fast charge separation and transportation in the hetero-structural nanomaterials can greatly boost photocatalytic H_2 production.

4. Conclusion

In summary, Ag_2S/CdS nanocomposites with high hydrogen evolution ability are successfully synthesized through a hydrothermal and subsequent *in situ* ion exchange method. The best photocatalytic activity of H_2 production of 777.3 μmol h^{-1} g^{-1} in lactic acid solution was achieved for Ag_2S/CdS nanocomposite with Ag_2S content ratio of 5.0%. The preeminent photocatalytic activity is mainly attributed to the driving force provided by the potential decline at the heterojunction interface, which can promote the photoinduced electrons directionally transfer from CdS NWs to Ag_2S NPs to participate in the HER. Meanwhile, benefitting from the narrow band gap of Ag_2S, the light absorption of the samples extends from visible light to infrared light, meaning their efficient light utilization efficiency. Furthermore, the photocatalytic mechanism of the Ag_2S/CdS nanocomposite is investigated in detail. Thus, this work sheds light on the synthesis of CdS-based nanocomposites for environmental and energetic applications.

Author contributions

Congrong Lu: conceptualization, data curation, investigation, formal analysis. Shiwen Du: methodology, data curation, writing-original draft. Yanfei Zhao: supervision, data curation, software. Qi wang: conceptualization, investigation, resources, methodology. Kuankuan Ren: supervision, visualization, software. Chunhe Li: conceptualization, formal analysis, funding acquisition, writing-review & editing. Weidong Dou: validation, resources, funding acquisition, project administration.

Conflicts of interest

The authors declare that they have no known competing financial interests or personal relationships that could have appeared to influence the work reported in this paper.

Acknowledgements

The authors are thankful for the support of the Natural Science Foundation of Zhejiang Province, China (Grant No. LQ21B030005 and LY19F040005) and Postdoctoral Science Foundation, China (No. 2021M692459).

References

1 A. Naldoni, M. Altomare, G. Zoppellaro and N. Liu, Photocatalysis with reduced TiO_2: From black TiO_2 to cocatalyst-free hydrogen production, *ACS Catal.*, 2019, **9**, 345–364.

2 W. Xing, W. Tu, Z. Han, Y. Hu, Q. Meng and G. Chen, Template-induced high-crystalline g-C_3N_4 nanosheets for enhanced photocatalytic H_2 evolution, *ACS Energy Lett.*, 2018, **3**, 514–519.

3 C. Li, H. Wang, S. B. Naghadeh, J. Z. Zhang and P. Fang, Visible light driven hydrogen evolution by photocatalytic reforming of lignin and lactic acid using one-dimensional NiS/CdS nanostructures, *Appl. Catal., B*, 2018, **227**, 229–239.

4 S. Xiao, W. Dai, X. Liu, D. Pan, H. Zou and G. Li, Microwave-induced metal dissolution synthesis of core–Shell copper nanowires/ZnS for visible light photocatalytic H_2 evolution, *Adv. Energy Mater.*, 2019, **9**, 1900775.

5 C. Li, S. Yi and D. Chen, Oxygen vacancy engineered $SrTiO_3$ nanofibers for enhanced photocatalytic H_2 production, *J. Mater. Chem. A*, 2019, **7**, 17974–17980.

6 Z. Tang, B. Han, C. Han and Y. Xu, One dimensional CdS based materials for artificial photoredox reactions, *J. Mater. Chem. A*, 2017, **5**, 2387–2410.

7 W. Li, K. Fang, Y. Zhang, Z. Chen, L. Wang and Y. Bu, Fabrication of 1D/2D CdS/CoS_x direct Z-scheme photocatalyst with enhanced photocatalytic hydrogen evolution performance, *Int. J. Hydrogen Energy*, 2020, **46**, 9351–9359.

8 J. Li, X. Liu and J. Zhang, Smart assembly of sulfide heterojunction photocatalysts with well-defined interfaces for direct Z-Scheme water splitting under visible light, *ChemSusChem*, 2020, **13**, 2996–3004.

9 X. L. Yin, L. L. Li, W. J. Jiang, Y. Zhang, X. Zhang, L. J. Wan and J. S. Hu, MoS_2/CdS Nanosheets-on-nanorod heterostructure for highly efficient photocatalytic H_2 generation under visible light irradiation, *ACS Appl. Mater. Interfaces*, 2016, **8**, 15258–15266.

10 W. Yu, J. Yin, Y. Li, B. Lai, T. Jiang, Y. Li, H. Liu, J. Liu and C. Guo, Ag_2S quantum dots as an infrared excited photocatalyst for hydrogen production, *ACS Appl. Mater. Interfaces*, 2019, **2**, 2751–2759.

11 X. Li, D. Shen, C. Liu, J. Li, Y. Zhou, X. Song, P. Huo and H. Wang, Fabricated rGO-modified Ag_2S nanoparticles/g-C_3N_4 nanosheets photocatalyst for enhancing photocatalytic activity, *J. Colloid Interface Sci.*, 2019, **554**, 468–478.

12 S. Zhao, J. Wu, Y. Xu, X. Zhang, Y. Han and H. Xing, CdS/Ag_2S/g-C_3N_4 ternary composites with superior photocatalytic performance for hydrogen evolution under visible light irradiation, *Dalton Trans.*, 2021, **50**, 3253–3260.

13 L. Zhang, P. Li, L. Feng, X. Chen, J. Jiang and S. Zhang, Synergetic Ag_2S and ZnS quantum dots as the sensitizer and recognition probe: A visible light-driven photoelectrochemical sensor for the "signal-on" analysis of mercury (II), *J. Hazard. Mater.*, 2020, **387**, 121715.

14 T. Kosmala, D. Mosconi, G. Giallongo, G. A. Rizzi and G. Granozzi, Highly efficient MoS_2/Ag_2S/Ag photoelectrocatalyst obtained from a recycled DVD surface, *ACS Sustainable Chem. Eng.*, 2018, **6**, 7818–7825.

15 H. Jia, W. He, W. G. Wamer, X. Han, B. Zhang and S. Zhang, Generation of reactive oxygen species, electrons/holes, and photocatalytic degradation of Rhodamine B by photoexcited CdS and Ag_2S micro-nano structures, *J. Phys. Chem. C*, 2014, **118**, 21447–21456.

16 H. Wang, S. B. Naghadeh, C. Li, L. Ying, A. Allen and J. Z. Zhang, Enhanced photoelectrochemical and photocatalytic activities of CdS nanowires by surface modification with MoS_2 nanosheets, *Sci. China Mater.*, 2018, **602**, 1–12.

17 H. Zhang, B. Wei, L. Zhu, J. Yu, W. Sun and L. Xu, Cation exchange synthesis of ZnS-Ag_2S microspheric composites with enhanced photocatalytic activity, *Appl. Surf. Sci.*, 2013, **270**, 133–138.

18 C. Li, S. Du, H. Wang, S. B. Naghadeh, A. L. Allen, X. Lin, G. Li, Y. Liu, H. Xu, C. He, J. Z. Zhang and P. Fang, Enhanced visible-light-driven photocatalytic hydrogen generation using $NiCo_2S_4$/CdS nanocomposites, *Chem. Eng. J.*, 2019, **378**, 122089.

19 B. M. Al-shehri, M. Shkir, T. M. Bawazeer, S. Alfaify and M. S. Hamdy, A rapid microwave synthesis of Ag_2S nanoparticles and their photocatalytic performance under UV and visible light illumination for water treatment applications, *Phys. E*, 2020, **121**, 114060.

20 T. Di, B. Cheng, W. Ho, J. Yu and H. Tang, Hierarchically CdS–Ag_2S nanocomposites for efficient photocatalytic H_2 production, *Appl. Surf. Sci.*, 2019, **470**, 196–204.

21 L. Liu, Y. Qi, J. Hu, Y. Liang and W. Cui, Efficient visible-light photocatalytic hydrogen evolution and enhanced photostability of core@shell Cu_2O@g-C_3N_4 octahedra, *Appl. Surf. Sci.*, 2015, **351**, 1146–1154.

22 D. H. Ortgies, Á. L. García-villalón, M. Granado, S. Amor, E. M. Rodríguez, D. A. Harrisson, J. Yao, J. Rubio-retama and D. Jaque, Infrared fluorescence imaging of infarcted hearts with Ag_2S nanodots, *Nano Res.*, 2019, **12**, 749–757.

23 B. Shi, Y. Qi and L. Tian, Fabrication of Ag_2S quantum dots sensitized CdSe photoelectrodes and its photoelectric performance, *Mater. Chem. Phys.*, 2020, **240**, 122177.

24 Y. Zhang, X. Li, J. Shen, Z. Chen, S. Cao, T. Li and F. Xu, Rechargeable Mg batteries based on a Ag_2S conversion cathode with fast solid-state Mg^{2+} diffusion kinetics, *Dalton Trans.*, 2019, **48**, 14390–14397.

25 W. Zhen, X. Ning, B. Yang, Y. Wu, Z. Li and G. Lu, The enhancement of CdS photocatalytic activity for water splitting *via* antiphotocorrosion by coating Ni_2P shell and removing nascent formed oxygen with artificial gill, *Appl. Catal., B*, 2017, **221**, 243–257.

26 S. Du, X. Lin, C. Li, G. Li, B. Zheng, Y. Liu, P. Fang, X. Lin, C. Li, G. Li, B. Zheng, Y. Liu, H. Xu and P. Fang, $CoSe_2$ modified Se-decorated CdS nanowire Schottky heterojunctions, *Chem. Eng. J.*, 2020, **339**, 124431.

27 Z. Liu, G. Liu and X. Hong, Influence of surface defects and palladium deposition on the activity of CdS nanocrystals for photocatalytic hydrogen production, *Wuli Huaxue Xuebao*, 2019, **35**, 215–222.

28 Z. Shao, X. Meng, H. Lai, D. Zhang, X. Pu, C. Su and H. Li, Coralline-like Ni_2P decorated novel tetrapod-bundle $Cd_{0.9}Zn_{0.1}S$ ZB/WZ homojunctions for highly efficient visible-light photocatalytic hydrogen evolution, Chinese, *J. Catal.*, 2021, **42**, 439–449.

29 Z. Zhang, R. Wang, X. Yue, S. Qiu and S. Yi, A novel architecture of dandelion-like Mo_2C/TiO_2 heterojunction photocatalysts towards high-performance photocatalytic hydrogen production from water splitting, *J. Mater. Chem. A*, 2017, **5**, 10591–10598.

30 L. Cheng, Y. Wang, Y. Li, Y. Shen, Y. Zhen, Z. Xing and L. Lin, Efficient CO_2 electroreduction on Ag2S nanodots modified CdS nanorods as cooperative catalysts, *ChemCatChem*, 2021, **200237**, 1161–1164.

31 Y. Xin, Z. Li, W. Wu, B. Fu and Z. Zhang, Pyrite FeS_2 sensitized TiO_2 nanotube photoanode for boosting near-infrared light photoelectrochemical water splitting, *ACS Sustainable Chem. Eng.*, 2016, **4**, 6659–6667.

32 B. He, C. Bie, X. Fei, B. Cheng, J. Yu, W. Ho, A. A. Al-Ghamdi and S. Wageh, Enhancement in the photocatalytic H_2 production activity of CdS NRs by Ag_2S and NiS dual cocatalysts, *Appl. Catal., B*, 2021, **288**, 119994.

33 T. Di, B. Cheng, W. Ho, J. Yu and H. Tang, Hierarchically CdS–Ag_2S nanocomposites for efficient photocatalytic H_2 production, *Appl. Surf. Sci.*, 2019, **470**, 196–204.

34 S. Wang, C. Ren, H. Tian, J. Yu and M. Sun, MoS_2/ZnO van der Waals heterostructure as a high-efficiency water splitting photocatalyst: A first-principles study, *Phys. Chem. Chem. Phys.*, 2018, **20**, 13394–13399.

35 K. Ren, J. Yu and W. Tang, Two-dimensional ZnO/BSe van der waals heterostructure used as a promising

photocatalyst for water splitting: A DFT study, *J. Alloys Compd.*, 2020, **812**, 152049.

36 C. Du, J. Tian and X. Liu, Effect of intrinsic vacancy defects on the electronic properties of monoclinic Ag_2S, *Mater. Chem. Phys.*, 2020, **249**, 122961.

37 Y. Luo, S. Wang, K. Ren, J. Chou, J. Yu, Z. Sun and M. Sun, Transition-metal dichalcogenides/$Mg(OH)_2$ van der Waals heterostructures as promising water-splitting photocatalysts: A first-principles study, *Phys. Chem. Chem. Phys.*, 2019, **21**, 1791–1796.